ELSEVIER

Engineering Analysis with Boundary Elements 23 (1999) 35–49

ENGINEERING ANALYSIS *with* BOUNDARY ELEMENTS

Analytical formulas for a 2-D crack tip singular boundary element for rectilinear cracks and crack growth analysis

M. Denda*, Y.F. Dong

Rutgers University, Mechanical and Aerospace Engineering Department, 98 Brett Road, Piscataway, NJ 08854-8058, USA

Abstract

Simple analytical formulas for the displacement, traction, and stress intensity factor for a 2-D crack tip singular boundary element are developed using the continuous distribution of dislocation dipoles and Chebyshev polynomials. The known $\sqrt{r}$ crack tip opening displacement and the $1/\sqrt{r}$ stress singularity at the crack tip is mathematically built into the formulas. In the boundary element implementation the crack tip singular element is placed locally at each crack tip on top of the ordinary non-singular crack elements that cover the entire crack surface. Within the constraint of the rectilinear approximation, any curvilinear cracks can be modeled, including center and edge cracks. Although the quarter-point element is accurate and easy to use, it does not provide the analytical formula for the stress intensity factor which is the key feature of the proposed method. The performance of the crack tip singular element is compared against other crack elements that incorporate the crack tip singularity analytically. A numerical result is given for a crack growth problem where repeated update of the crack shape and calculation of the stress intensity factor are required as the crack grows in a curvilinear path.

Keywords: Boundary element method; Crack tip singular element; Analytical stress intensity formula; Dislocation dipole distribution

1. Introduction

Among several elastic two-dimensional crack modeling strategies by the boundary element method (BEM), there exist the multi-domain formulation [1,2], the stress formulation with regularization [3], and the dual boundary element method [4,5]. For each formulation options are available such as building in the crack tip stress singularity [6,7], using the quarter-point boundary element [1,8], and strategically refining the near-crack-tip non-singular elements. Further details on elastic crack analysis by the boundary element method are given in [9,10], which include the Green's function method [2,11].

In the Green's function method the fundamental solution that satisfies the traction-free crack surface condition is used. The Green's function incorporates both the crack tip opening displacement ($\sqrt{r}$) and the singular stress ($1/\sqrt{r}$) behaviors correctly. However, it is limited to a straight single crack. The method of introducing the crack tip stress singularity either by the singular interpolation function or by the quarter-point boundary element is versatile, but the crack tip opening displacement is not correctly modeled. The method of singular integral equations [12–17], which uses the numerical solution procedure developed by Erdogan et al. [13], can be applied to multiple curvilinear crack problems and has the same mathematical consistency as the Green's function method. In this method the continuous distribution of dislocation densities is used to represent the gradient of the crack opening displacement which, for center cracks, is interpolated by the product of Chebyshev polynomials and the associated singular weight function with $1/\sqrt{r}$ singularity at crack tips. This powerful technique, originally limited to problems with simple geometry such as the infinite and semi-infinite domains, was subsequently coupled with the BEM to incorporate more complex boundary geometry [18,19].

Liu et al. [20] have proposed an alternative integral equation approach that uses the displacement discontinuity (i.e., the crack opening displacement) instead of the dislocation density (i.e., the gradient of the crack opening displacement). Since the crack opening displacement is zero at crack tips and continuous at kinks, the ordinary BEM integration scheme can be adopted instead of the sophisticated integration scheme required for the treatment of the gradient of the crack opening displacement which exhibits $1/\sqrt{r}$ singularity at crack tips and weaker singularity at kinks.

Denda and Dong [21] have developed analytical integration formulas for the displacement discontinuity distribution

* Corresponding author

0955-7997/99/$ - see front matter
PII: S0955-7997(98)00059-9

along straight cracks which exhibit both the correct crack tip stress and crack tip opening displacement behaviors. The availability of these analytical formulas eliminates the need for the special quadrature formulas for the numerical integration of the singular integrals arising in 2-D straight crack problems. The interpolation scheme used by Denda and Dong [21], as in the standard singular integral method, is based on p-type refinement for which the order of orthogonal polynomials is varied but the element size, spanning the whole extent of a crack, is fixed. Because of this, the element may be identified as a whole crack singular element. To be specific, the crack opening displacement is interpolated by the product of a function with the $\sqrt{r}$ crack tip behavior and orthogonal polynomials. Since a center crack has two crack tips and an edge crack has one, different formulas must be used for the two types of cracks even though the local behavior at each crack tip is identical.

The primary objective of this paper is to develop a set of analytical formulas for a local crack tip singular element so that it can be embedded at an arbitrary crack tip regardless of the configuration of the whole crack. In the boundary element implementation the crack tip singular element is placed locally at each crack tip on top of the ordinary non-singular crack elements that cover the entire crack surface. Within the constraint of the rectilinear approximation, any curvilinear cracks can be modeled, including center and edge cracks. Although the quarter-point element is accurate and easy to use, it does not provide an analytical formula for the stress intensity factor. Consequently an indirect procedure, such as the evaluation of the *J*-integral, must be used to calculate the stress intensity factor numerically. The proposed analytical formula for the stress intensity factor overcomes this disadvantage of the quarter-point element. Further, the performance of the crack tip singular element is compared against the whole crack elements that incorporate the known crack tip singularity. A numerical result is given for a crack growth problem where repeated update of the crack shape and calculation of the stress intensity factor are required as the crack grows in a curvilinear path.

2. Singularity solutions of elasticity

2.1. Point force and point force distribution

In this paper the coordinate point (ξ_x, ξ_y), the displacement (u_x, u_y) and the traction (t_x, t_y) in two dimensions are expressed by complex variables $\xi = \xi_x + i\xi_y$, $u = u_x + iu_y$ and $t = t_x + it_y$, respectively, where $i = \sqrt{-1}$ is a pure imaginary number. Consider a point force $f = f_x + if_y$ acting at a point ξ of an infinite plane. The resulting displacement at a point $z = x + iy$ can be obtained in complex variable form [22,23] using the Muskhelishvili formalism [24] of plane elasticity, with the result

$$u^{(f)}(z,\ \xi) = -\frac{\kappa f}{2\pi\mu(\kappa+1)}\mathrm{Re}[\ln(z-\xi)] + \frac{\bar{f}}{4\pi\mu(\kappa+1)}\frac{(z-\xi)}{\overline{(z-\xi)}}, \tag{1}$$

where μ is the shear modulus, and κ is given by $\kappa = 3 - 4\nu$ in plane strain and $\kappa = (3-\nu)/(1+\nu)$ in plane stress in terms of Poisson's ratio ν. The symbol Re indicates the real part and an overbar the complex conjugate of a complex variable. The solution does not depend on the choice of the branch cut for $\ln(z-\xi)$ because only the real part of it is used in Eq. (1). The traction at z on a line segment with the unit normal $n = n_x + in_y = \mathrm{e}^{i\alpha}$ is given by

$$t^{(f)}(z,\ \xi) = -\frac{\mathrm{e}^{-i\alpha}}{2\pi(\kappa+1)}\left\{ f\left[\frac{\mathrm{e}^{i2\alpha}}{(z-\xi)} + \frac{\kappa}{\overline{(z-\xi)}}\right] + \bar{f}\left[\frac{\mathrm{e}^{i2\alpha}}{\overline{(z-\xi)}} + \frac{(z-\xi)}{\overline{(z-\xi)}^2}\right]\right\}.$$

Consider a point force distribution on a smooth arc L with density $T(\xi)$. The corresponding displacement at a point z is obtained by integrating Eq. (1) over the arc, with the result

$$u(z) = -\frac{1}{4\pi\mu(\kappa+1)} \times \int_L \left\{ 2\kappa\mathrm{Re}\left[\ln(z-\xi)\right]T(\xi) - \frac{(z-\xi)}{\overline{(z-\xi)}}\overline{T(\xi)}\right\}\mathrm{d}s, \tag{2}$$

where $\mathrm{d}s = |\mathrm{d}\xi|$ represents the infinitesimal arc length. The traction at z is given by

$$t(z) = -\frac{\mathrm{e}^{-i\alpha}}{2\pi(\kappa+1)}\int_L \left\{ \left[\frac{\mathrm{e}^{i2\alpha}}{(z-\xi)} + \frac{\kappa}{\overline{(z-\xi)}}\right]T(\xi) + \left[\frac{\mathrm{e}^{i2\alpha}}{\overline{(z-\xi)}} + \frac{(z-\xi)}{\overline{(z-\xi)}^2}\right]\overline{T(\xi)}\right\}\mathrm{d}s. \tag{3}$$

2.2. Dislocation dipole and dislocation dipole distribution

For an edge dislocation at ξ with constant Burgers vector $b = b_x + ib_y$, the displacement solution in the complex variable form is given in [22,23] by

$$u^{(b)}(z,\ \xi) = -\frac{ib}{2\pi(\kappa+1)}\left[\kappa\ln(z-\xi) - \overline{\ln(z-\xi)}\right] - \frac{i\bar{b}}{2\pi(\kappa+1)}\frac{(z-\xi)}{\overline{(z-\xi)}}, \tag{4}$$

where the branch cut for $\ln(z-\xi)$ is taken along the line of displacement discontinuity. The traction at z on a line segment with the unit normal $n = n_x + in_y = \mathrm{e}^{i\alpha}$ is

given by

$$t^{(b)}(z,\ \xi) = -\frac{i\mathrm{e}^{-i\alpha}}{2\pi\mu(\kappa+1)}\left\{b\left[\frac{\mathrm{e}^{i2\alpha}}{(z-\xi)} - \frac{1}{\overline{(z-\xi)}}\right] - \bar{b}\left[\frac{\mathrm{e}^{i2\alpha}}{\overline{(z-\xi)}} + \frac{(z-\xi)}{\overline{(z-\xi)}^2}\right]\right\}. \tag{4}$$

We introduce a dislocation dipole as a constant dislocation distribution over an infinitesimal segment $\mathrm{d}\xi$ at point ξ. It is constructed by a pair of edge dislocations with opposite Burgers vectors $-b$ and b located at ξ and $\xi + \mathrm{d}\xi$, respectively. The resulting displacement and traction are given by

$$\mathrm{d}u^{(b)}(z,\ \xi) = \frac{i}{2\pi(\kappa+1)}\left\{b\left[\frac{\kappa\mathrm{d}\xi}{(z-\xi)} - \frac{\mathrm{d}\bar{\xi}}{\overline{(z-\xi)}}\right] + \bar{b}\left[\frac{\mathrm{d}\xi}{\overline{(z-\xi)}} - \frac{(z-\xi)}{\overline{(z-\xi)}^2}\mathrm{d}\bar{\xi}\right]\right\}, \tag{5}$$

and

$$\mathrm{d}t^{(b)}(z,\ \xi) = -\frac{i\mathrm{e}^{-i\alpha}}{2\pi\mu(\kappa+1)}\left\{b\left[\frac{\mathrm{e}^{i2\alpha}}{(z-\xi)^2}\mathrm{d}\xi - \frac{1}{\overline{(z-\xi)}^2}\mathrm{d}\bar{\xi}\right] - \bar{b}\left[\frac{\mathrm{e}^{i2\alpha}}{\overline{(z-\xi)}^2}\mathrm{d}\bar{\xi} - \frac{1}{(z-\xi)^2}\mathrm{d}\xi + 2\frac{(z-\xi)}{\overline{(z-\xi)}^2}\mathrm{d}\bar{\xi}\right]\right\}. \tag{6}$$

For an arbitrary distribution $B(\xi)$ of dislocation dipoles over a smooth arc L the magnitude of the displacement jump varies along the arc. The solution is obtained by integrating Eqs. (5) and (6) along the arc L, with the result

$$u(z) = \frac{i}{2\pi(\kappa+1)}\int_L\left\{\left[\frac{\kappa B(\xi)}{(z-\xi)} + \frac{\overline{B(\xi)}}{\overline{(z-\xi)}}\right]\mathrm{d}\xi - \left[\frac{B(\xi)}{\overline{(z-\xi)}} + \frac{(z-\xi)}{\overline{(z-\xi)}^2}\overline{B(\xi)}\right]\mathrm{d}\bar{\xi}\right\},$$

$$t(z) = -\frac{i\mathrm{e}^{-i\alpha}}{2\pi\mu(\kappa+1)}\left\{\int_L\left[\frac{\mathrm{e}^{i2\alpha}}{(z-\xi)^2}B(\xi) + \frac{1}{\overline{(z-\xi)}^2}\overline{B(\xi)}\right]\mathrm{d}\xi - \int_L\left[\frac{\mathrm{e}^{i2\alpha}}{\overline{(z-\xi)}^2}\overline{B(\xi)} + \frac{1}{(z-\xi)^2}B(\xi) + 2\frac{(z-\xi)}{\overline{(z-\xi)}^2}\overline{B(\xi)}\right]\mathrm{d}\bar{\xi}\right\}, \tag{7}$$

for the displacement and traction, respectively.

3. Crack modeling

Consider a body R with its boundary ∂R subject to the traction $t = t_x + it_y$ and the displacement $u = u_x + iu_y$. According to a physical interpretation [25] of Somigliana's identity, the displacement field in this body is obtained by assuming that the region R is embedded in an infinite medium and that ∂R, which is simply a line marked out in the infinite domain, is covered by a continuous distribution of point forces with density t and by a continuous distribution of dislocation dipoles with Burgers vector u.

We discretize and approximate the original boundary by a set of straight lines, $\partial\tilde{R} = \sum_{j=1}^{M} L_j$, where $L_j = \xi_j\xi_{j+1}$ ($j = 1, 2, \ldots, M$) is the jth boundary element. On each boundary element we approximate the density functions T and B by quadratic Lagrange interpolation polynomials in the form

$$T(\xi) = \sum_{\alpha=1}^{3}\varphi_\alpha(\xi)T_\alpha,\ B(\xi) = \sum_{\alpha=1}^{3}\varphi_\alpha(\xi)B_\alpha, \tag{8}$$

where T_α and B_σ are nodal values of the density functions and $\varphi_\alpha(\xi)$ ($\alpha = 1, 2, 3$) are quadratic shape functions. For the straight boundary element the boundary integrals are evaluated analytically [21], providing the explicit BEM formulas in complex variables for the displacement and traction formulations of the BEM.

Next, consider a crack along a directed arc L with upper and lower surfaces L^+ and L^-, respectively. It is subject to tractions t^+ and t^- and displacements u^+ and u^- on the two surfaces. The boundary element formulation for this crack results in layers along L of point forces and dislocation dipoles with densities $t_{\mathrm{cr}} = t^+ + t^-$ and $\delta = u^+ - u^-$, respectively. In this paper we assume $t_{\mathrm{cr}} = 0$ and model cracks by the continuous distribution of dislocation dipoles. Following the standard procedure of boundary element discretization, we can approximate the crack by a collection of straight elements so that curvilinear cracks are modeled by rectilinear cracks. If the singular elements are not introduced, the crack opening displacement is approximated by the polynomial interpolation (Eq. (8)). We evaluate the traction on one (i.e., upper or lower) of the crack surfaces to establish a system of traction boundary equations, which will be solved for the unknown crack opening displacement. This system of traction equations is coupled with another system of boundary equations if a non-crack boundary is present in the body. Since the crack tip singularity is not built into the interpolation, extra efforts must be made to refine the mesh near the crack tips and to extract the stress intensity factor indirectly.

In Sections 3.1 and 3.2 we present alternative techniques for crack modeling using the whole crack singular elements and the crack tip singular element, each of which models the crack tip singularity analytically and provides an analytical formula for the stress intensity factor.

3.1. Whole crack singular elements for straight cracks

3.1.1. Center cracks

For a straight center crack of length $2a$, select the origin of the coordinate system at its center with the x-axis along the crack. If we rescale the coordinate system by a factor of $1/a$ (i.e., $X = x/a$, $Y = y/a$ and $Z = z/a = X + iY$) so that the crack lies in the interval $(-1, +1)$, and interpolate the crack

opening displacement by

$$B(X)=\frac{i\mu}{\pi(\kappa+1)}\sqrt{1-X^2}\sum_{m=1}^{p}\delta^{(m)}U_{m-1}(X), \tag{9}$$

where $U_{m-1}(X)$ is the Chebyshev polynomial of the second kind, then the integrals in Eq. (7) can be evaluated analytically [21]. The explicit formula for the displacement is given by

$$u(z)=\frac{i}{2(\kappa+1)}\sum_{m=1}^{p}\Big[\Big\{\kappa T^{(m)}(Z)-\overline{T^{(m)}(Z)}\Big\}\delta^{(m)} + m(Z-\bar{Z})\overline{U^{(m-1)}(Z)\delta^{(m)}}\Big], \tag{10}$$

and for the traction by

$$t(z)=\frac{\mu}{a(\kappa+1)}\sum_{m=1}^{p} m\Big[\Big\{e^{i\alpha}U^{(m-1)}(Z)+e^{-i\alpha}\overline{U^{(m-1)}(Z)}\Big\}\delta^{(m)} + \Big\{(e^{-i\alpha}-e^{i\alpha})\overline{U^{(m-1)}(Z)} + e^{-i\alpha}\frac{\bar{Z}-Z}{\bar{Z}^2-1}\Big\{(m+1)\overline{T^{(m)}(Z)}-\overline{U^{(m)}(Z)}\Big\}\Big\}\overline{\delta^{(m)}}\Big]. \tag{11}$$

where

$$T^{(m)}(Z)=\left(Z-\sqrt{Z^2-1}\right)^m (m\geq 0),$$

$$U^{(m-1)}(Z)=-\frac{\left(Z-\sqrt{Z^2-1}\right)^m}{\sqrt{Z^2-1}} (m\geq 0). \tag{12}$$

Note that the known crack tip behavior of the center crack is built into the formulas through the complex-valued term $\sqrt{Z^2-1}$, which takes different values (i.e., $\pm i\sqrt{1-X^2}$) as we approach the crack toward the upper and lower surfaces (i.e., $Z\rightarrow X^{\pm}$). These formulas can be used for the solution of a center crack in an infinite body subject to traction t^+ and t^- (with $t_{cr}=0$) and the only unknown is the crack opening displacement $\delta=u^+-u^-$. The unknown crack opening displacement is determined with the help of the traction equation on the crack surface

$$(t_X+it_Y)^{\pm}(X)=\pm\frac{2\mu}{(\kappa+1)a}\sum_{m=1}^{p}m\delta^{(m)}U_{m-1}(X)\ (|X|\leq 1), \tag{13}$$

which is set to t^+ (or t^-) at collocation points; evaluation on only one side of the crack surfaces is sufficient. Once the crack opening displacement is determined, the stress intensity factor is given by

$$K(\pm 1)=K_{\mathrm{I}}(\pm 1)+iK_{\mathrm{II}}(\pm 1) =\frac{2\mu i}{\kappa+1}\sqrt{\frac{\pi}{a}}\sum_{m=1}^{p}(\pm 1)^{m+1}m\overline{\delta^{(m)}}, \tag{14}$$

where $K_{\mathrm{I}}(\pm 1)$ and $K_{\mathrm{II}}(\pm 1)$ are Mode I and II stress intensity factors at $X=\pm 1$, respectively. Note that there is no need to obtain the stress intensity factors by extrapolation or other indirect methods such as the J-integral.

3.1.2. Edge cracks

For a straight edge crack of length $2a$, also select the x-axis along the crack with its origin at the center of the crack and rescale the coordinate system so that the crack lies in the interval $(-1, +1)$ on the new X-axis. The crack tip and mouth are located at $X=+1$ and $X=-1$, respectively. We interpolate the crack opening displacement by

$$B(X)=\frac{i\mu}{\pi(\kappa+1)}(1-X)^{\alpha}(1+X)^{\beta}\sum_{m=1}^{p}\delta^{(m)}P_{m-1}^{(\alpha,\beta)}(X) + \frac{i\mu}{\pi(\kappa+1)}\sum_{n=1}^{q}\Delta^{(n)}(1-X)^n, \tag{15}$$

where the first and the second terms in the right-hand side are called the singular and regular terms, respectively, $P_m^{(\alpha,\beta)}(X)$ is the Jacobi polynomial, and $\delta^{(m)}$ and $\Delta^{(n)}$ are the crack opening displacement coefficients. The singular term captures the crack tip opening behavior at $X=+1$ with the choice of $\alpha=1/2$, while the regular term is needed to provide non-zero crack opening at the crack mouth $X=-1$. The value of β in the singular term is selected such that no stress singularity arises at the crack mouth; the convenient but arbitrary choice is $\beta=3/2$ which has been shown [26] to have negligible effects on the stress intensity factor. Analytical evaluation of integrals in Eq. (7) with the interpolation (Eq. (15)) was performed by Denda and Dong [21] with displacement, traction and stress intensity factor formulas corresponding to the singular part in (15) given by

$$u(z)=\frac{i}{2(\kappa+1)}\sum_{m=1}^{p}\Big[\Big\{\kappa R^{(m)}(Z)-\overline{R^{(m)}(Z)}\Big\}\delta^{(m)} + 2m(Z-\bar{Z})\overline{G^{(m-1)}(Z)\delta^{(m)}}\Big], \tag{16}$$

$$t(z)=\frac{2\mu}{a(\kappa+1)}\sum_{m=1}^{p}m\Big[\Big\{e^{i\alpha}G^{(m-1)}(Z)+e^{-i\alpha}\overline{G^{(m-1)}(Z)}\Big\}\delta^{(m)} + \Big\{(e^{-i\alpha}-e^{i\alpha})\overline{G^{(m-1)}(Z)}+\frac{(m+1)}{2}e^{-i\alpha}\frac{\bar{Z}-Z}{\bar{Z}^2-1} \times\Big[\overline{R^{(m)}(Z)}+\frac{4}{\alpha+\beta+2m} \times\Big\{(\alpha-\beta)\overline{G^{(m-1)}(Z)}+(\alpha+\beta-2)\overline{G^{(m)}(Z)}\Big\}\Big]\Big\}\overline{\delta^{(m)}}\Big], \tag{17}$$

$$K(\pm 1)=K_{\mathrm{I}}(\pm 1)+iK_{\mathrm{II}}(\pm 1) =\frac{2\mu i}{\kappa+1}2^{\beta+\alpha}\sqrt{\frac{\pi}{a}}\sum_{m=1}^{p}mP_m^{(\alpha-1,\beta-1)}(1)\overline{\delta^{(m)}}, \tag{18}$$

where

$$R^{(m)}(z) = -\frac{1}{\sin \pi\alpha}\Big\{P_{m-1}^{(\alpha,\beta)}(z)(z-1)^{\alpha}(z+1)^{\beta} - 2^{\alpha+\beta}p_{m-1+\alpha+\beta}^{(-\alpha,-\beta)}(z)\Big\},$$

$$G^{(m-1)}(z) = -\frac{1}{\sin \pi\alpha}\Big\{P_{m}^{(\alpha-1,\beta-1)}(z)(z-1)^{\alpha-1}(z+1)^{\beta-2} - 2^{\alpha+\beta-2}p_{m-2+\alpha+\beta}^{(1-\alpha,1-\beta)}(z)\Big\}. \quad (19)$$

The treatment of the regular part in Eq. (15) follows that for the ordinary polynomial interpolation for the BEM. The essential part of edge crack problems is the presence of a non-crack boundary and inevitable coupling with the BEM. Especially important is the requirement of displacement compatibility. The displacement jump experienced by the boundary element nodes across the crack mouth must be equal to the crack opening displacement there. For the boundary elements that intersect a crack, discontinuous elements may be used to relax the requirement of displacement compatibility at the crack mouth. The collocation points can be selected arbitrarily except to avoid the crack tip and crack mouth, where the traction contribution from the regular part in (15) becomes unbounded.

The crack opening displacement can be interpolated either by the non-singular element or by the whole crack singular element based on orthogonal polynomials. Multiple non-singular elements must be used to simulate the crack tip behavior accurately, with an advantage that they can model rectilinear cracks. On the other hand, a single whole crack singular element using Chebyshev polynomials can model a straight center crack. The use of the singular element based on Jacobi polynomials is more flexible. Since this element has the singularity at its one end only it can model either an entire edge crack or only the near-crack-tip straight portion of any crack provided that the non-zero crack opening displacement is properly taken into consideration by regular terms such as those in Eq. (15). Dong and Denda [27] proposed to adopt the Jacobi polynomial whole crack singular element as the crack tip element for arbitrarily shaped cracks consisting of straight segments. After discretizing a crack into multiple crack elements, they have implemented this singular crack element at the crack tip as shown in Fig. 1(a) and (b). The size of this crack tip element may be large if a sufficient number of Jacobi polynomial terms in (15) is used. For example, we can select either a long crack segment AB (Fig. 1(a)) or a shorter near-tip segment AA_1 (Fig. 1(b)) as the extent of the whole crack singular element; the longer element requires more terms in the interpolation (15) than the shorter one. The crack opening displacement for the rest of the crack elements is interpolated by ordinary polynomials given by Eq. (8). Note that the crack tip singular element introduced in the next section uses a Chebyshev polynomial over a short crack tip element AA_1 (Fig. 1(b)) and that the non-zero crack opening within the crack tip element is interpolated by the ordinary polynomial interpolation (8) instead of the second term in (15).

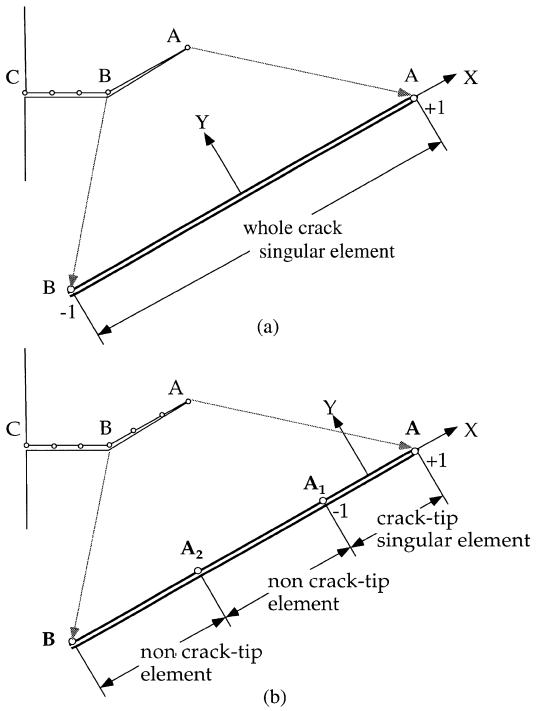

Fig. 1. (a) Whole crack singular element; (b) crack tip singular element.

3.2. Crack tip singular element

In the following we propose to use the Chebyshev polynomial whole crack singular element as a crack tip singular element. The first step is to discretize a crack into multiple crack elements, as shown in Fig. 1(b), and interpolate the crack opening displacement in each element by the polynomial interpolation function (8); the crack opening displacement is taken care of by the polynomial (or non-singular) elements first. In the second step we modify the crack tip element AA_1 by superposing the Chebyshev polynomial whole crack singular element $AA_1^{(s)}$ on top of the existing non-singular crack tip element $AA_1^{(ns)}$. Note that for a center crack we need to embed two singular crack tip elements, one at each crack tip. If we select the size of the crack tip element small compared to the crack length, it is sufficient to take only one term of the interpolation (Eq. (9)). This results in a set of simple formulas. The crack opening contribution from this crack tip element is interpolated by

$$B(X) = \frac{i\mu}{\pi(\kappa+1)}\sqrt{1-X^2}\,\delta^{(1)}U_0(X) \quad (20)$$

in the local non-dimensional coordinate system attached to the crack tip element. The displacement and traction contributions of this crack tip singular element are

given by

$$u(z)=\frac{i}{2(\kappa+1)}\Big[\Big\{\kappa T^{(1)}(Z)-\overline{T^{(1)}(Z)}\Big\}\delta^{(1)} + (Z-\bar{Z})\overline{U^{(0)}(Z)\delta^{(1)}}\Big] \tag{21}$$

and

$$t(z)=\frac{\mu}{a(\kappa+1)}\Big[\Big\{e^{i\alpha}U^{(0)}(Z)+e^{-i\alpha}\overline{U^{(0)}(Z)}\Big\}\delta^{(1)} + \Big\{(e^{-i\alpha}-e^{i\alpha})\overline{U^{(0)}(Z)} + e^{-i\alpha}\frac{\bar{Z}-Z}{\bar{Z}^2-1}\Big\{\overline{2T^{(1)}(Z)}-\overline{U^{(1)}(Z)}\Big\}\Big\}\overline{\delta^{(1)}}\Big], \tag{22}$$

where

$$T^{(1)}(Z)=Z-\sqrt{Z^2-1},$$

$$U^{(m-1)}(Z)=-\frac{\left(Z-\sqrt{Z^2-1}\right)^m}{\sqrt{Z^2-1}}\ (m=1,\ 2). \tag{23}$$

The stress intensity factor contribution is given by

$$K(\pm 1)=K_{\mathrm{I}}(\pm 1)+iK_{\mathrm{II}}(\pm 1)=\frac{2\mu i}{\kappa+1}\sqrt{\frac{\pi}{a}}\overline{\delta^{(1)}}, \tag{24}$$

where a is half the crack tip element length.

Notice dual tip singularities at ends A and A_1 of the singular crack tip element in Fig. 1(b); i.e., the stress singularity at the two ends is $1/\sqrt{r}$. While the singularity at end A of the element reflects the true crack tip singular behavior, the singularity at the other end A_1 is spurious. It is true that the effect of the spurious singularity at A_1 becomes more pronounced for very small crack tip element size and it might seem that the use of the Jacobi polynomial whole crack singular element, with the only singularity at end A, is a more natural choice. Despite these initial concerns, the suggested use of the formulas (20)–(24) for the crack tip singular element, with sensible selection of its size coupled with the use of the discontinuous element, provides an excellent scheme for modeling rectilinear cracks. Consider the traction formulation of the BEM on an ordinary non-crack boundary using the polynomial interpolation functions (8) for the boundary variables. It is found that at the end points of each element the stress behaves like $1/r$, where r is the distance measured from the end point. This is an artificial singularity originating from the discretization of the BEM and does not represent any physically existing singularities. Although these singularities are canceled between two adjacent elements if the element slope and the traction are continuous, they persist otherwise. Use of the discontinuous elements, for which the collocation points are selected away from the end nodes, is the standard BEM procedure to alleviate this situation. Meanwhile, on the crack surface the traction equations arising from the non-singular crack elements present exactly the same singularity

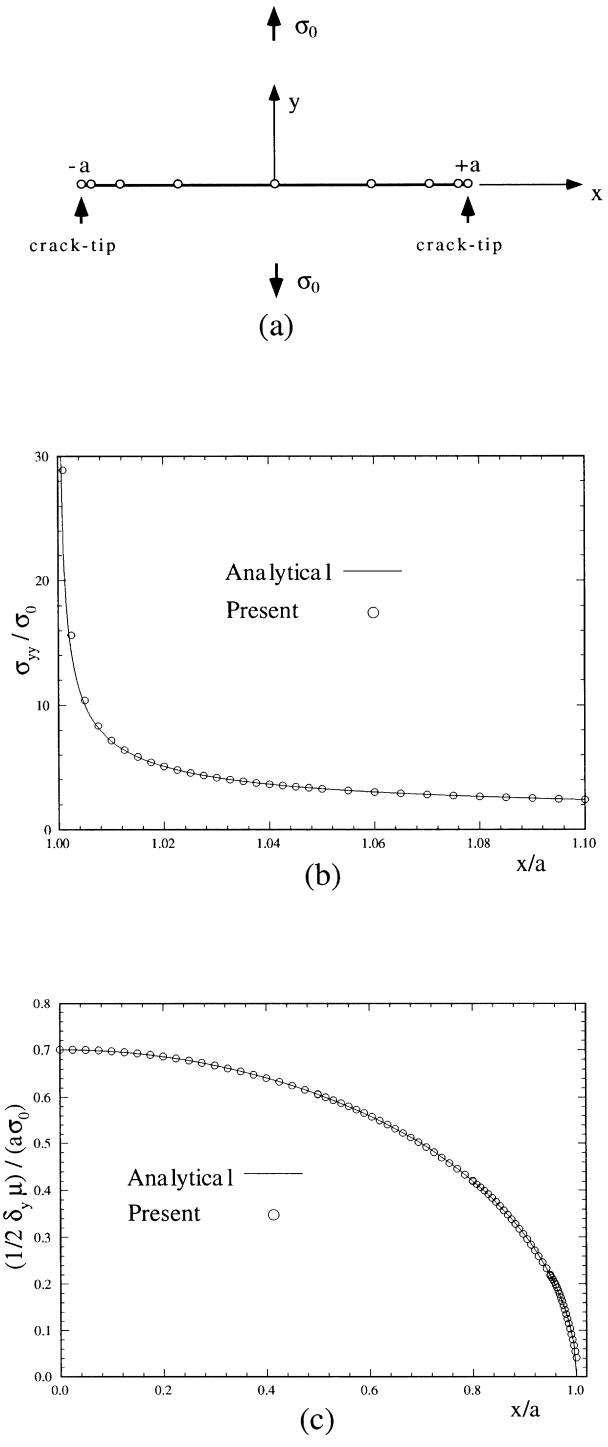

Fig. 2. (a) The boundary element mesh for a crack in an infinite body under uniaxial tension. (b) Stress σ_{yy} ahead of the crack tip along the crack axis of the center crack. (c) Crack opening displacement δ_y (actually $1/2\delta_y$).

configuration as explained above for non-crack elements, which forces us to use the discontinuous elements on the crack.

We take advantage of this situation in the introduction of the singular crack tip elements. Consider a collocation point of the crack tip element a distance r away from the end point

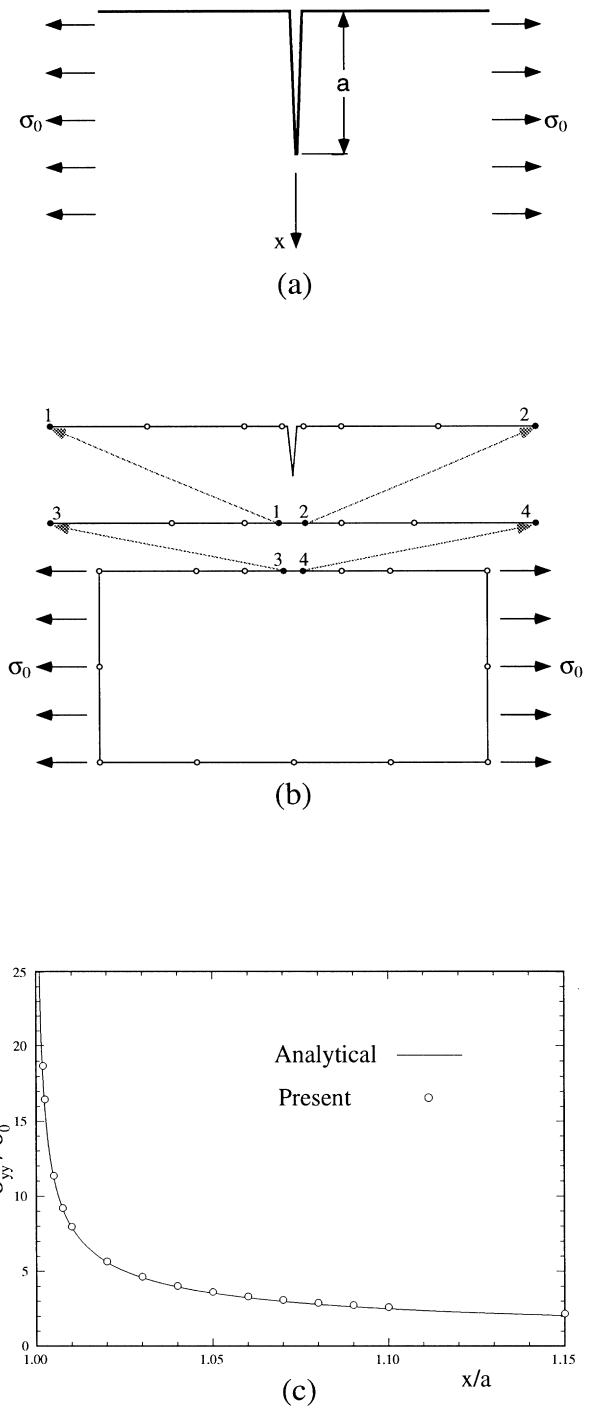

Fig. 3. (a) An edge crack in a semi-infinite plane under uniaxial tension. (b) The boundary element mesh for the non-crack boundary approximating the semi-infinite plane. (c) Stress σ_{yy} ahead of the crack tip along the crack axis of the edge crack.

A_1. Since $1/r$ is much larger than $1/\sqrt{r}$ for a small distance r, the effect of the spurious singularity $1/\sqrt{r}$ at A_1 is not numerically detected at the collocation point. Therefore, the use of the Chebyshev polynomial singular crack tip element is justified, with the provision that the collocation point is shifted from the end point A_1 by using the discontinuous boundary element. The suggested offset distance for the discontinuous element is between 1/40 and 1/20 of the element size.

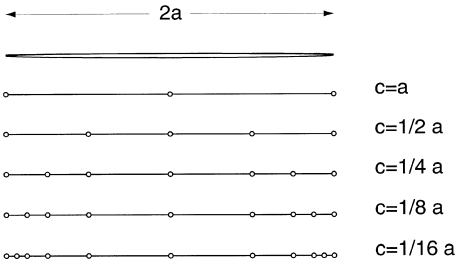

Fig. 4. Symmetric meshes tested for a center crack.

3.3. Numerical results

As mentioned earlier, the crack opening displacement is approximated by the polynomial (or non-singular) elements (Eq. (8)) first, followed by the singular crack tip elements that are embedded on top of the polynomial (non-singular) element at each crack tip. The accuracy of the numerical results depends not only on the crack tip singular elements but also on the selection of non-singular crack elements. Therefore, numerical results for crack problems based solely on these non-singular crack elements are reported first. Fig. 2(a) shows a boundary element mesh for a straight traction-free crack of length $2a$ in an infinite body under tension. The crack is divided into eight discontinuous crack elements and the crack opening displacement is approximated by the quadratic interpolation function (8); no crack tip singular elements are introduced. Fig. 2(b) and (c) show the distributions along the crack axis of the stress σ_{yy} ahead of the crack tip and the crack opening displacement, respectively. The agreement of the present result with the analytical solution is excellent considering that only eight non-singular boundary elements are used in the analysis.

Fig. 3(a) and (b) show an edge crack in a semi-infinite plane under uniaxial tension and the mesh (with 26 elements) used for the non-crack boundary that progressively becomes coarser as we move away from the cracked region. The displacement boundary element method is used for the non-crack boundary and the traction boundary element method for the crack. The mesh for the crack is the same as for the center crack problem mentioned above. The distribution of the stress component σ_{yy} ahead of the crack along the crack axis is shown in Fig. 3(c), which is in excellent agreement with the analytical solution. Note that even without using the crack tip singular elements the numerical results are quite accurate; however, the stress intensity factors must be obtained through an extrapolation procedure, based on the crack opening displacement or the stress distribution ahead of the crack, which will provide an additional source of error.

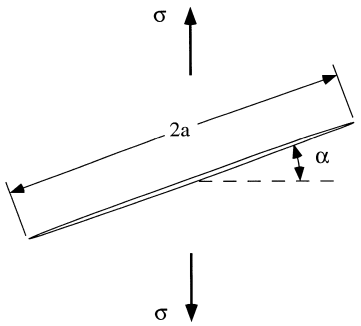

Fig. 5. An inclined center crack in an infinite plate in tension.

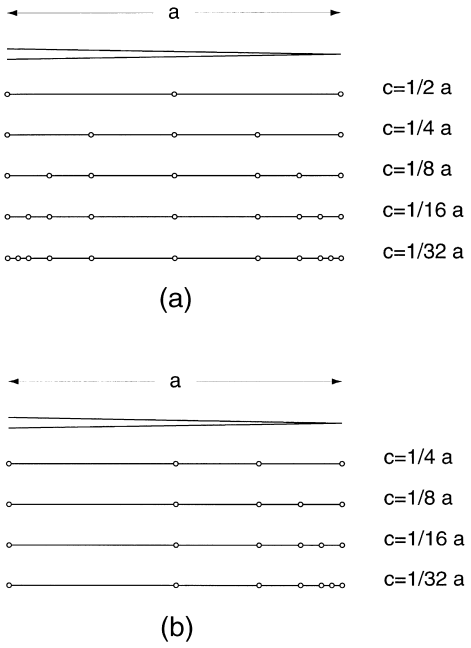

Fig. 6. (a) Symmetric and (b) asymmetric meshes tested for an edge crack.

We have performed a series of tests on the effects of the crack tip singular element size for basic configurations of center and edge cracks. For a center crack of length 2*a*, typical arrangements of crack elements used are shown in Fig. 4 with the size *c* of the crack tip element ranging from $c = a$ to $c = a/16$. The stress intensity factor results for an inclined center crack in an infinite region under tension, as shown in Fig. 5, are given in Table 1. For an edge crack of length *a*, we have tested sets of symmetrical and asymmetrical arrangements of crack elements, as shown in Fig. 6(a) and (b), respectively. The asymmetrical arrangement recognizes the absence of singularity at the crack mouth and adopts the arrangement used for one half of the center crack, while the symmetrical arrangement adopts that for the center crack without modification. The stress intensity factor results for an edge crack in a semi-infinite plane in tension, as shown in Fig. 3(a), are given in Table 2. Note

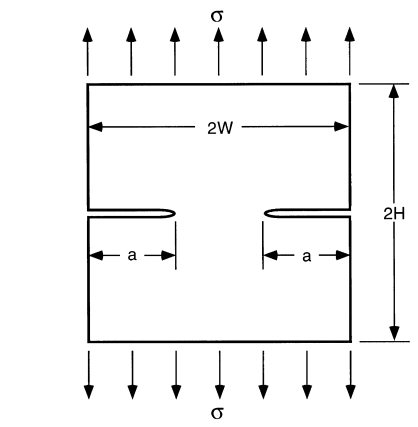

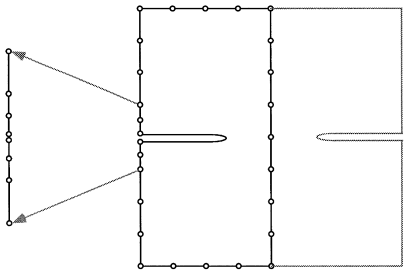

Fig. 7. (a) Double edge cracks in a plate in tension; (b) the mesh used.

Table 1
The effect of crack tip singular element size on the stress intensity factor of an inclined crack in an infinite plate under uniaxial tension (K_I^{anal} and K_{II}^{anal} are the analytical solutions)

	$\alpha = 0°$	$\alpha = 30°$		$\alpha = 45°$		$\alpha = 60°$	
	K_I/K_I^{anal}	K_I/K_I^{anal}	K_{II}/K_{II}^{anal}	K_I/K_I^{anal}	K_{II}/K_{II}^{anal}	K_I/K_I^{anal}	K_{II}/K_{II}^{anal}
$c = a$	1.010	1.010	1.010	1.010	1.010	1.010	1.010
$c = a/2$	1.006	1.006	1.006	1.006	1.006	1.006	1.006
$c = a/4$	1.003	1.003	1.003	1.003	1.003	1.003	1.003
$c = a/8$	1.001	1.001	1.001	1.001	1.001	1.001	1.001
$c = a/16$	1.000	1.000	1.000	1.000	1.000	1.000	1.000
$c = a/32$	0.999	0.999	0.999	0.999	0.999	0.999	0.999
$c = a/64$	0.999	0.999	0.999	0.999	0.999	0.999	0.999

Table 2
The effect of crack tip singular element size on the stress intensity factor of an edge crack in a semi-infinite plate under uniaxial tension (K_I^{anal} is the analytical solution)

	Symmetrical mesh	Asymmetrical mesh
	K_I/K_I^{anal}	K_I/K_I^{anal}
$c = a/2$	1.010	1.010
$c = a/4$	1.006	1.007
$c = a/8$	1.004	1.004
$c = a/16$	1.002	1.003
$c = a/32$	1.001	1.002
$c = a/64$	1.000	1.002
$c = a/128$	1.000	1.001
$c = a/256$	0.999	1.001

that, for edge cracks, there is no need to refine the mesh near the crack mouth and the asymmetrical arrangement provides accurate stress intensity factor results,

The next three numerical examples have been obtained by the Chebyshev polynomial singular crack tip element as well as by the whole crack singular elements introduced in Section 3.1 so that the two sets of results can be compared. For the non-crack boundary, identical boundary element mesh has been used for the two methods. The numerical result of the stress intensity factors for double edge cracks in a rectangular plate, as shown in Fig. 7(a), are given in Table 3 along with the solution by Bowie [29]. Exploiting the symmetry of the problem, only one half of the plate was analyzed, as is shown in Fig. 7(b) which shows the boundary element mesh (with 30 elements) used for the non-crack boundary. First we have used the Jacobi polynomial whole crack singular element along the crack; the number of singular and regular terms used for the interpolation (Eq. (15)) is $m = 2$ and $n = 9$. For the crack tip singular element, the size of the crack tip element is $c = a/32$ with the asymmetric arrangement of the crack elements shown in Fig. 6(b). The accuracy of the Bowie solution is unknown.

The second example is a kinked crack in a semi-infinite plate under uniaxial tension, as shown in Fig. 8(a). The non-crack boundary of the semi-infinite body is modeled by 34 nonhomogeneous elements consisting of a gradually refined mesh (Fig. 8(b)) as we approach the crack mouth. Twelve crack elements (six for each of the straight segments AB and

Table 3
Stress intensity factors for double edge cracks in a rectangular plate under tension, where $\eta(a/W,\ H/W) = K_I/\{\sigma\sqrt{2W\tan(\pi a/2W)}\}$ (WCE = whole crack element, CTE = crack tip element)

a/W	$\eta(a/W, H/W)$ $H/W = 1$		
	[29]	WCE	CTE
0.1	1.13	1.11	1.13
0.2	1.13	1.13	1.16
0.4	1.16	1.16	1.19
0.8	1.01	1.02	1.05

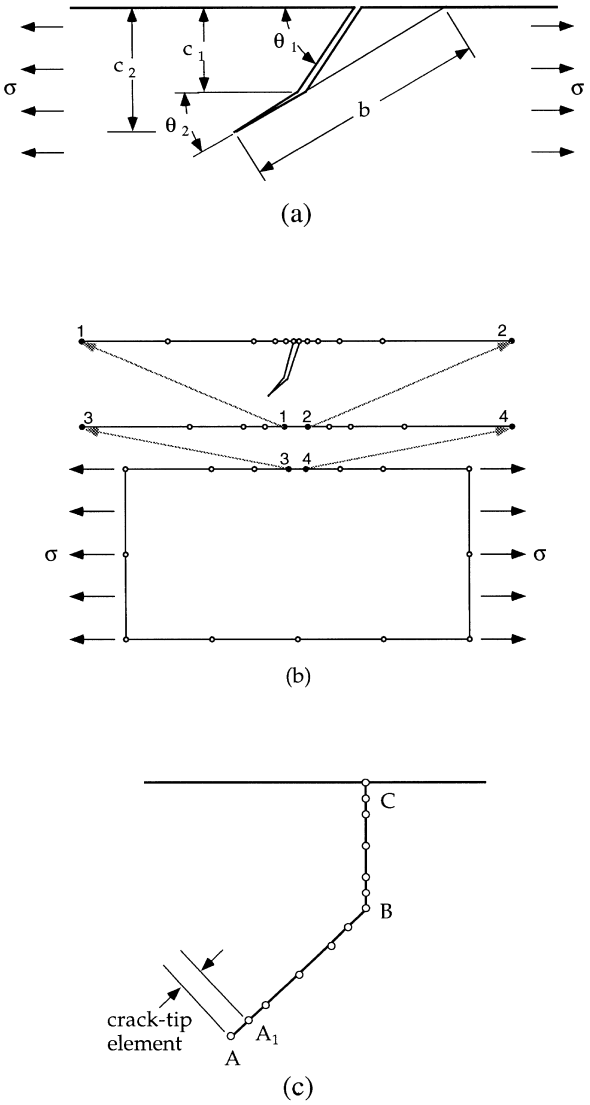

Fig. 8. (a) A kinked crack in a semi-infinite plate in tension; (b) mesh for non-crack boundary and (c) crack elements for the kinked crack with crack tip element AA_1.

BC) are introduced along the kinked crack, as shown in Fig. 8(c); the size of the singular crack tip element AA_1 is 1/8 of the near crack tip segment AB. The same problem has been calculated by the Jacobi polynomial whole crack singular element as follows. The crack elements, with the exception of the one at the crack tip, along with the mesh and the interpolation scheme for the non crack boundary are unchanged. The only difference exists in the interpolation scheme of the crack tip element AA_1, where the crack opening displacement is interpolated by Eq. (15) with $m = 2$ and $n = 3$. The numerical results for the stress intensity factors are given in Table 4 along with the analytical solution given in the stress intensity handbook [30]. The only available analytical solution, in the handbook, does not seem to be accurate enough for our comparison since its result, $K_{II} = 0$ for the case $\theta_1 = 45°$ and $\theta_2 = 90°$, is obviously incorrect.

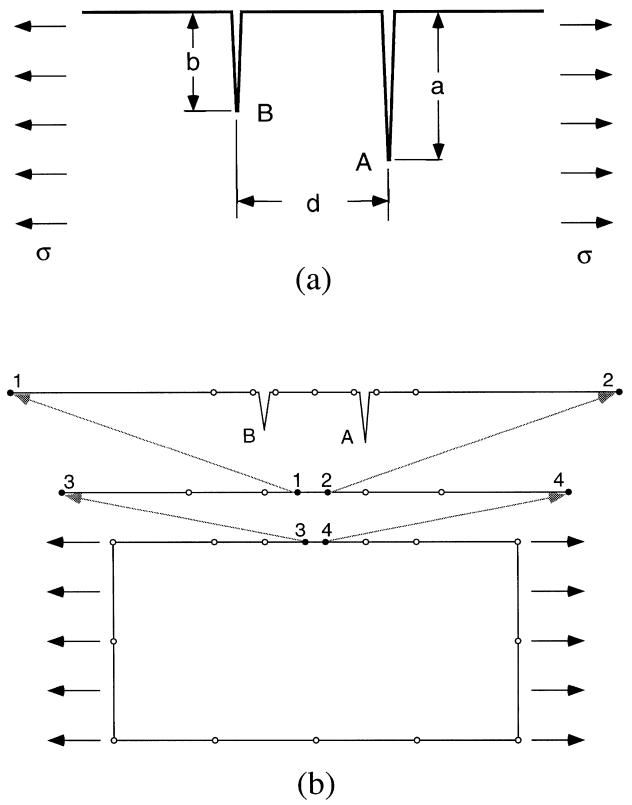

Fig. 9. (a) Two parallel edge cracks in a semi-infinite plate in tension; (b) the mesh used for non-crack boundary.

Fig. 9(a) shows two edge cracks in a semi-infinite plate subject to tension. The accuracy of the solution given in the handbook [30] is known to be within 0.1%. Fig. 9(b) shows a non-crack boundary mesh (with 26 elements) that progressively becomes coarser as we move away from the cracked region. First, we have used the Jacobi polynomial whole crack singular element; the number of singular and regular terms used for the interpolation (15) is $m = 3$ and $n = 8$. The crack tip singular element used has the size $c_i = a_i/8$ with the symmetrical mesh in Fig. 6(a) for each of the two cracks with length a_i. The stress intensity factor results are listed in Tables 5 and 6. For the two sets of numerical results, the majority of the values stay within 0.1% of the handbook values, whose accuracy is reported to be 0.1%.

In summary, for the suggested crack tip singular element to provide accurate stress intensity factors (typically less than 1% error) a sensible selection of the crack tip element size and the arrangement of the rest of the non-singular crack elements are essential. We recommend the length of the crack tip element to be between 1/32 and 1/8 (typically 1/16) of the near-crack-tip segment which is one half of a straight center crack or the whole of a straight edge crack. Selecting the crack tip element size outside of this range, either too big or too small, will result in errors bigger than 1% in the stress intensity factor.

The proposed scheme does not model the singularities present at kinks of rectilinear cracks. When a crack suddenly kinks, such as in the model analyzed by Lo [28], the singularity at the kink could interact with the singularity at the crack tip if the size of the kink is extremely small. The crack growth analysis presented in Section 4 faces this sudden kink, which occurs at the first increment of the crack extension. We have found that, if the crack increment size is of the same order as the size of the crack tip element immediately prior to the crack extension, the effect of the singularity at the sudden kink becomes unimportant as far as the stress intensity factor calculation is concerned.

4. Crack growth analysis

4.1. Crack growth criterion

According to the criterion of local symmetry [31,32], a crack in a non-uniform stress field, if it grows smoothly, takes a path in the direction for which the local crack tip stress field is of Mode I (i.e., $K_{\mathrm{II}}^{\mathrm{local}} = 0$). Various crack growth criteria, including the maximum hoop stress [33], maximum energy release rate [34–36], minimum strain energy density [37] and maximum dilatational strain energy density [38], are consistent with the criterion of local symmetry in the contra-positive sense that if $K_{\mathrm{II}} \neq 0$ at the crack tip the crack extends with an abrupt change in direction. With the exception of the maximum energy release rate

Table 4
The stress intensity factor for a kinked edge crack in a semi-infinite plate under tension (WCE = whole crack element, CTE = crack tip element)

θ_2	θ_1	c_2	c_1	$K_{\mathrm{I}}/\sigma\sqrt{\pi b}$			$K_{\mathrm{II}}/\sigma\sqrt{\pi b}$		
				[30]	WCE	CTE	[30]	WCE	CTE
45°	90°	1.0	0.25	0.703	0.691	0.706	−0.365	−0.359	−0.365
			0.50	0.704	0.692	0.706	−0.365	−0.359	−0.365
			0.75	0.705	0.692	0.706	−0.366	−0.359	−0.366
			0.90	0.707	0.693	0.706	−0.359	−0.352	−0.359
90°	45°	1.0	0.25	1.121	1.101	1.124	0.0	−1.330D−04	−6.252D−05
			0.50	1.121	1.101	1.123	0.0	−1.732D−03	−1.541D−03
			0.75	1.122	1.103	1.124	0.0	−6.635D−03	−6.274D−03
			0.90	1.121	1.100	1.124	0.0	−8.492D−03	−6.274D−03

Table 5
Stress intensity factors for two edge cracks in the semi-infinite plate under tension: Mode I with $F_{IA} = K_{IA}/\sigma\sqrt{\pi a}$, $F_{IB} = K_{IB}/\sigma\sqrt{\pi b}$ (WCE = whole crack element, CTE = crack tip element)

b/a	d/a	0.5		1.0		2.0	
		F_{IA}	F_{IB}	F_{IA}	F_{IB}	F_{IA}	F_{IB}
1.0	[30]	0.817	0.817	0.854	0.854	0.911	0.911
	WCE	0.825	0.825	0.854	0.854	0.909	0.909
	CTE	0.821	0.821	0.858	0.858	0.914	0.914
0.75	[30]	1.066	0.407	1.015	0.644	1.005	0.827
	WCE	1.054	0.405	1.015	0.642	1.003	0.823
	CTE	1.074	0.403	1.021	0.643	1.008	0.827
0.5	[30]	1.118	0.118	1.094	0.418	1.071	0.738
	WCE	1.119	0.114	1.093	0.414	1.067	0.737
	CTE	1.125	0.111	1.100	0.413	1.075	0.739
0.25	[30]	1.122	−0.042	1.118	0.214	1.109	0.659
	WCE	1.122	−0.042	1.117	0.212	1.104	0.644
	CTE	1.128	−0.050	1.124	0.208	1.112	0.677

criterion, all the other criteria are based on the crack tip field prior to the extension of the cracks and are called prior field criteria. In general, however, these criteria do not seem to predict drastically different crack growth directions. The crack growth criterion used in this section is the maximum hoop stress criterion, which is the most commonly used criterion.

The maximum hoop stress criterion postulates that the crack will grow in the direction normal to the maximum hoop stress $\sigma_{\theta\theta}$ at the crack tip. For a crack under mixed Mode I and Mode II loading, the criterion uses the crack tip asymptotic singular stress field given by the polar components

$$\sigma_{\theta\theta} = \frac{1}{\sqrt{2\pi r}}\cos\frac{\theta}{2}\left[K_I\cos^2\frac{\theta}{2} - \frac{3}{2}K_{II}\sin\theta\right],$$

$$\sigma_{r\theta} = \frac{1}{2\sqrt{2\pi r}}\cos\frac{\theta}{2}\left[K_I\sin\theta + K_{II}(3\cos\theta - 1)\right] \tag{25}$$

and σ_{rr}, where K_I and K_{II} are the Mode I and II stress intensity factors. The criterion implies that along the crack growth direction the $\sigma_{\theta\theta}$ is maximum and the shear stress $\sigma_{r\theta}$ is zero, which leads to an equation

$$K_I\sin\theta_c + K_{II}(3\cos\theta_c - 1) = 0. \tag{26}$$

Since the crack growth direction established this way is locally in Mode I, the quantity

$$K_{Ieq} = \sqrt{2\pi r}\sigma_{\theta\theta}$$

gives the equivalent Mode I stress intensity factor [39]. The criterion for crack extension initiation is thus given by

$$K_{Ieq} = \cos\frac{\theta_c}{2}\left[K_I\cos^2\frac{\theta_c}{2} - \frac{3}{2}K_{II}\sin\theta_c\right] = K_{Ic}, \tag{27}$$

where K_{Ic} is the critical stress intensity factor. The key role played by the crack tip singular element developed in this paper is to provide the local stress intensity factors K_I^{local} and K_{II}^{local} directly and accurately without relying on other indirect methods such as the J-integral as used in [39]. The direction of incremental crack path is determined by Eq. (26) and the equivalent Mode I stress intensity factor by Eq. (27). In the crack growth analysis the increment of crack extension is approximated by a straight line. An algorithm that effectively controls the crack increment size is proposed below.

Table 6
Stress intensity factors for two edge cracks in the semi-infinite plate under tension: Mode II with $F_{IIA} = K_{IIA}/\sigma\sqrt{\pi a}$, $F_{IIB} = K_{IIB}/\sigma\sqrt{\pi b}$ (WCE = whole crack element, CTE = crack tip element)

b/a	d/a	0.5		1.0		2.0	
		F_{IIA}	F_{IIB}	F_{IIA}	F_{IIB}	F_{IIA}	F_{IIB}
1.0	WCE	−0.155	0.155	−0.132	0.132	−0.092	0.092
	CTE	−0.159	0.159	−0.133	0.133	−0.093	0.093
0.75	WCE	−0.052	0.177	−0.072	0.159	−0.059	0.095
	CTE	−0.047	0.176	−0.072	0.160	−0.060	0.096
0.5	WCE	0.003	0.096	−0.024	0.145	−0.029	0.080
	CTE	−0.008	0.096	−0.024	0.146	−0.030	0.081
0.25	WCE	0.004	0.024	−0.003	0.092	−0.008	0.050
	CTE	0.033	0.023	−0.003	0.092	−0.008	0.052

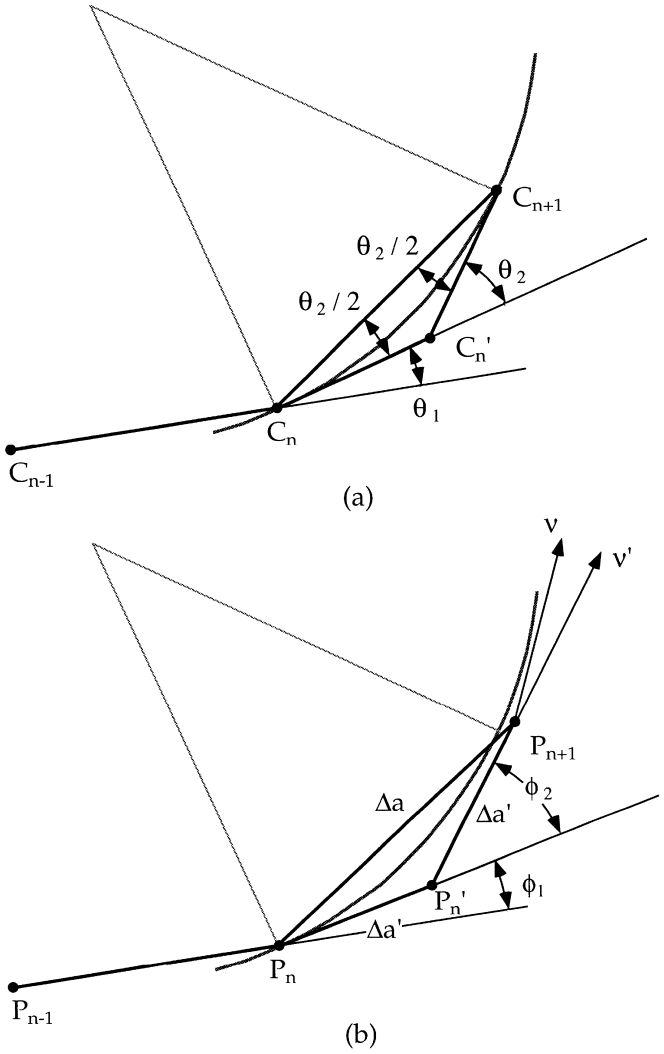

Fig. 10. Incremental crack extension direction for (a) ideal crack path and (b) actual crack path obtained in numerical analysis.

Fig. 10(a) represents the ideal scenario of the crack growth analysis. Let us assume, in Fig. 10(a), that C_n and C_{n+1} are the true crack tip positions. For a small crack increment the crack path is described by a circular arc and the crack extension can be approximated either by the single secant C_nC_{n+1} or by two successive tangents C_nC_n' and $C_n'C_{n+1}$. Fig. 10(b) shows the rectilinear crack path obtained in the numerical analysis. Assume that, after the nth crack increment, under certain applied load, the current crack tip is located at P_n as shown in Fig. 10(b). We will describe the procedure of determining the new position P_{n+1} of the crack tip. With the crack tip at P_n, calculate the direction of the crack extension increment using Eq. (26) and grow the crack by an amount $\Delta a'$ to point P′ in Fig. 10(b). With the new crack tip at P_n' repeat the incremental crack growth to grow the crack by $\Delta a'$ to point P_{n+1}. In addition to the crack increment path $P_nP_n'P_{n+1}$ (tangential path) just obtained we introduce a second increment path P_nP_{n+1} (secant path), both of which are used to predict the next crack increment directions, ν and ν', using (26). As the crack increment size is reduced, the difference between these two directions is expected to diminish to satisfy the condition

$$|\nu - \nu'| \leq \epsilon \tag{28}$$

where ϵ is the tolerance limit. If the condition (28) is not satisfied, then we reduce the crack increment size $\Delta a'$ appropriately to repeat the above procedure until the new crack tip location P_{n+1} is determined. The secant P_nP_{n+1} will then be selected as the new extended crack path.

4.2. Numerical results

We have performed an incremental crack growth analysis for a cruciform cracked plate subject to biaxial tension T_1 and T_2, represented in Fig. 11. This problem was analyzed by Portela et al. [39] earlier by the dual boundary element method. The plate has square arms of length $L = 80$ cm, and an edge crack of length $a = 20$ cm, inclined at 45° from the horizontal direction, is located at one of the interior corners.

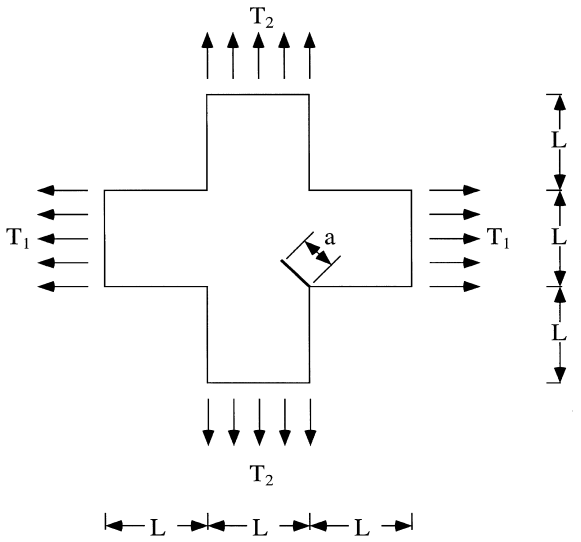

Fig. 11. Cruciform plate in biaxial tension containing an edge crack.

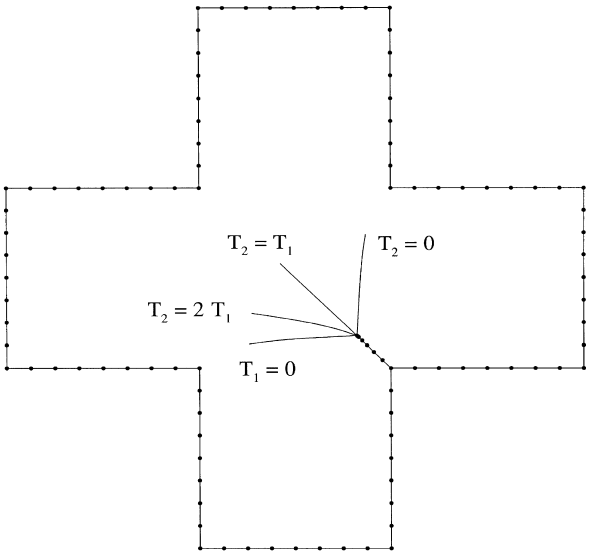

Fig. 12. Crack paths for the cruciform cracked plate problem.

The loading cases considered are given by (1) $T_2 = 0$, $T_1 \neq 0$, (2) $T_2 = T_1$, (3) $T_2 = 2T_1$, and (4) $T_1 = 0$, $T_2 \neq 0$. Fig. 12 shows the boundary element mesh (7 elements on the crack and 96 elements on the non-crack boundary) and the four crack paths generated by the analysis.

In each analysis the size of the initial crack tip element was chosen to be 1/16 of the initial edge crack length. Since the analytic solutions for the initial and subsequent crack configurations are unavailable, an additional auxiliary crack tip element with half the size of the adopted crack tip element was used to check the accuracy; at each incremental stage of the crack growth analysis these two stress intensity factor values remained consistently within 1%. The initial crack increment size was selected equal to 1.05 times the size of the crack tip element, $c_0 = 0.5$ cm, of the initial crack. Similarly, the subsequent crack increment size was selected to be 1.05 times the current crack tip element size. With this effort and the value of $\epsilon = 0.1°$, the condition (28) was always satisfied and no iteration was necessary to reduce the crack increment size. To gain numerical efficiency, it is desirable to increase the crack increment size as much as possible, but this will reduce the numerical accuracy. The factor 1.05 for the crack increment size was selected on the basis of this consideration. Each crack growth analysis was carried until the total crack length reached 65 cm. Fig. 13 shows the equivalent Mode I stress intensity factor (K_{Ieq}) history for the four loading cases. For each loading the value of K_{Ieq} is normalized by the value K^0_{Ieq} calculated with the initial crack. Cases $T_2 = 0, T_1 \neq 0$ and $T_1 = 0$, $T_2 \neq 0$ give the identical stress intensity history, as expected.

The advantage of the present scheme is its capability of adjusting the crack increment size. Another important factor in the determination of the crack increment size is the balance between the size of the crack tip element and the crack increment size. In order to achieve reliable numerical results, the crack increment size $\Delta a'$ needs to be kept comparable to that for the current crack tip element. While an accurate simulation of the crack growth requires the use of small crack increments, too small an increment size will lead to an approximation error, as discussed in Section 3.3. In addition, there always exists an incentive to save CPU time by increasing the crack increment size. The numerical example presented above is based on a crack growth analysis in which the size $\Delta a'$ is selected to be 1.05 times the current crack tip element size; this is a rather small size within the guide line. In this case the condition of Eq. (28) is always satisfied. The penalty for the use of such a smaller increment size is the longer CPU time, but the use of the analytical formulas for the crack tip singular element alleviates the situation drastically by reducing the CPU time. We have found that, when the increment size $\Delta a'$ of 2.0 times the current crack tip element size is used, the condition (28) is almost always violated and the increment size has to be reduced. It should be emphasized that, even when the actual crack growth is smooth and the changes between successive elements are small, the selection of large crack increment size could lead to a large discrepancy between two predicted crack directions, thus violating condition (28). So even if the angle change between successive elements could be of the same order as the angle difference tolerance of $\epsilon = 0.1°$ in Eq. (28), this condition still stands as an effective guideline in the determination of the crack increment size.

5. Concluding remarks

When the crack opening displacement in a crack tip element is interpolated by

$$B(X) = \frac{i\mu}{\pi(\kappa+1)}\sqrt{1-X^2}\,\delta^{(1)}$$

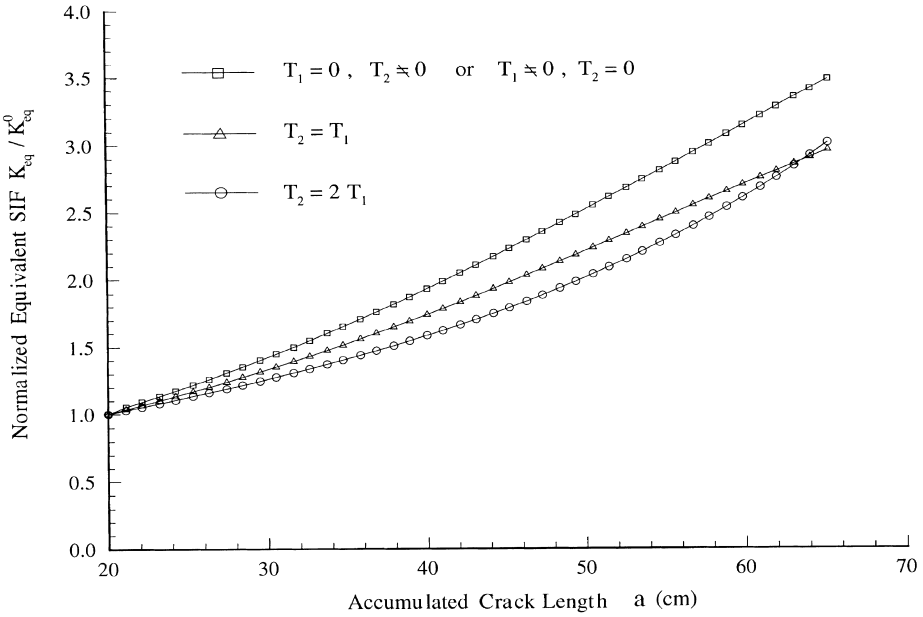

Fig. 13. Variation of the equivalent Mode I stress intensity factor along the crack path.

in the local non-dimensional coordinate system attached to the crack tip element, the displacement contribution of the crack tip element is given by

$$u(z) = \frac{i}{2(\kappa+1)}\left[\left\{\kappa T^{(1)}(Z) - \overline{T^{(1)}(Z)}\right\}\delta^{(1)} + (Z-\bar{Z})\overline{U^{(0)}(Z)\delta^{(1)}}\right],$$

where

$$T^{(1)}(Z) = \left(Z - \sqrt{Z^2-1}\right),$$

$$U^{(0)}(Z) = -\frac{\left(Z-\sqrt{Z^2-1}\right)}{\sqrt{Z^2-1}}.$$

The use of the crack tip singular element coupled with the ordinary boundary elements for crack problems for arbitrarily shaped finite bodies has been established. The direct and accurate determination of the stress intensity factors by the simple formula

$$K(\pm 1) = K_{\mathrm{I}}(\pm 1) + iK_{\mathrm{II}}(\pm 1) = \frac{2\mu i}{\kappa+1}\sqrt{\frac{\pi}{a}}\overline{\delta^{(1)}}$$

plays a key role in the crack analysis. With a judicious choice of the crack tip element size, the error of the stress intensity factor results has been confirmed, most of the time, to be within 1% on the basis of comparison with stress intensity handbook results. To demonstrate the simplicity and accuracy of the crack tip singular element, it has been applied to an incremental crack growth analysis with great success.

Acknowledgements

This work was supported by the FAA Center for Computational Modeling of Aircraft Structures at Rutgers University.

References

[1] Blandford GE, Ingraffea AR, Liggett JA. Two-dimensional stress intensity factor computations using the boundary element method. Int J Num Methods Eng 1981;17:387–404.
[2] Kuhn G. Numerische Behandlung von Mehrfachrissen in ebenen Scheiben. ZAMM 1981;61:105–106.
[3] Balas J, Sladek J, Sladek V. Stress analysis by boundary element methods. Amsterdam: Elsevier, 1989.
[4] Hong H, Chen J. Derivatives of integral equations of elasticity. J Eng Mech 1988;114(6):1028–1044.
[5] Portela A, Aliabadi MH. The dual boundary element method: effective implementation for crack problems. Int J Num Methods Eng 1992;33:1269–1287.
[6] Aliabadi MH. The evaluation of the stress intensity factors using the two-dimensional boundary element method. Technical Report EMR/10/2. Southampton: Engineering Materials Department, Southampton University, June 1985.
[7] Tanaka M, Itoh H. New crack elements for boundary element analysis of elastostatics considering arbitrary stress singularities. Appl Math Modelling 1987;11:357–363.
[8] Cruse TA, Wilson RB. Boundary integral equation method for elastic fracture mechanics analysis. Technical Report AFOSR–TR–780355. Pratt and Whitney Aircraft Group, 1977.
[9] Cruse TA. Boundary element analysis in computational fracture mechanics. Dordrecht: Kluwer, 1989.
[10] Aliabadi MH, Rooke DP. Numerical fracture mechanics Southampton: Computational Mechanics Publications and Dordrecht: Kluwer, 1991.
[11] Snyder MD, Cruse TA. Boundary integral equation analysis of cracked anisotropic plates. Int J Fract 1975;11:315–328.
[12] Savruk MP. Plane problems of the theory of elasticity for a multiply

connected area with holes and cracks (in Russian). Fiz-Khim Mekh Mater 1980;16(5):51–56.
[13] Erdogan F, Gupta GD, Cook TS. Numerical solution of singular integral equations. In: Sih GC, editor. Mechanics of fracture 1: methods of analysis and solutions of crack problems. Leyden: Noordhoff, 1973:368–425.
[14] Theocaris PS, Ioakimidis NI. Numerical integration method for the solution of singular integral equations. Quart Appl Math 1977;35: 173–183.
[15] Panasyuk VV, Savruk MP, Datsyshyn AP. A general method of solution of two-dimensional problems in the theory of cracks. Eng Fract Mech 1977;9:481–497.
[16] Barr DT, Cleary MP. Thermoelastic fracture solutions using distributions of singular influence functions—I: determining crack stress fields from dislocation distributions. Int J Solids Struct 1983;19(1): 73–82.
[17] Lam KY, Phua SP. Multiple crack interaction and its effect on stress intensity factor. Eng Fract Mech 1991;40(3):585–592.
[18] Sturt A, Nowell D, Hills DA. Application of the boundary element and dislocation density methods in plane crack problems. Eng Anal Bound Elem 1993;11:129–135.
[19] Sheng CF. Boundary element method by dislocation distribution. J Appl Mech 1987;54:105–109.
[20] Liu N, Altiero NJ, Sur U. An alternative integral equation approach applied to kinked cracks in finite plane bodies. Comput Methods Appl Mech Eng 1990;84:211–226.
[21] Denda M, Dong YF. Complex variable approach to the BEM for multiple crack problems. Comput Methods Appl Mech Eng 1997;141:247–264.
[22] Denda M. Complex variable Green's function representation of plane inelastic deformation in isotropic solids. Acta Mech 1988;72:205–221.
[23] Denda M. Formulation of the plastic source method for plane inelastic problems, part 1: Green's functions for plane inelastic deformation. Acta Mech 1988;75:93–109.
[24] Muskhelishvili N. Some basic problems of the mathematical theory of elasticity. Groningen: Noordhoff, 1958.
[25] Eshelby JD. The elastic field of a crack extending non-uniformly under general anti-plane loading. J Mech Phys Solids 1969;17:177–199.
[26] Dewynne SN, Hills DA, Nowell D. Calculation of the opening displacement of surface-breaking plane cracks. Comput Methods Appl Mech Eng 1992;97:321–331.
[27] Dong YF, Denda M. Computational modeling of elastic and plastic multiple cracks by the fundamental solutions. Finite Elem Anal Des 1996;23:115–132.
[28] Lo KK. Analysis of branched cracks. J Appl Mech 1978;45:797–802.
[29] Bowie OL. Rectangular tensile sheet with symmetric edge cracks. J Appl Mech 1964;31(2):208.
[30] Murakami Y et al. Stress intensity factor handbook. Oxford: Pergamon, 1987.
[31] Goldstein RV, Salganik RL. Brittle fracture of solids with arbitrary cracks. Int J Fract 1974;10(4):507–523.
[32] Cotterell B, Rice JR. Slightly curved or kinked cracks. Int J Fract 1980;16(2):155–169.
[33] Erdogan F, Sih GC. On the crack extension in plates under plane loading and transverse shear. J Basic Eng 1963;85:519–527.
[34] Palaniswamy K, Knauss WG. Propagation of a crack under general in-plane tension. Int J Fract Mech 1972;8:114–117.
[35] Hussain MA, Pu SL, Underwood S. Strain energy release rate for a crack under combined mode—I and —II. In: Fracture analysis. Philadelphia, PA: ASTM, 1974:2–28.
[36] Wu CH. Fracture under combined loads by maximum-energy-release-rate criterion. J Appl Mech 1978;45:553–558.
[37] Sih GC. Strain energy density factor applied to mixed-mode crack problems. Int J Fract 1974;10:305–321.
[38] Theocaris PS, Andrianopoulos NP. The Mises elastic–plastic boundary as the core region in fracture criteria. Eng Fract Mech 1982; 16(3):425–432.
[39] Portela A, Aliabadi MH, Rooke DP. Dual boundary element incremental analysis of crack propagation. Comput & Struct 1993;46(2): 237–247.